Tribological changes of tooth enamel-mullite/3Y-TZP couple in artificial saliva

Yanqi Huang
Central South University

Zhuan Li (lizhuan@csu.edu.cn)
Central South University https://orcid.org/0000-0003-3093-1941

Peng-fei Liu
Aalborg Universitet

Yan-meng Cheng
Central South University

Wen-jie Li
Central South University

Peng Xiao
Central South University

Yang Li
Central South University

Research Article

Keywords: Mullite/3Y-TZP, Tribological properties, Artificial saliva, Wear resistance

Posted Date: July 21st, 2020

DOI: https://doi.org/10.21203/rs.3.rs-45430/v1

Abstract

In-situ mullite toughened 3Y-TZP composite ceramic (mullite/3Y-TZP) with excellent mechanical properties was fabricated by gel-casting. The cytotoxicity of mullite/3Y-TZP was determined by both extract and direct contact methods, and the results indicated that mullite/3Y-TZP had no acute cytotoxicity. Furthermore, the tribological properties of the tooth enamel sliding against mullite/3Y-TZP in artificial saliva were investigated by using the pin-on-disk friction method. The friction coefficient (μ) between the two friction samples was about 0.464 with a stable friction process, and both of them showed slight wear. Analysis of the wear surface and debris demonstrated that the tooth enamel mainly suffered from fatigue wear accompanied by mild adhesive wear, while mullite/3Y-TZP showed slight abrasive wear. This result indicated that mullite/3Y-TZP had good wear resistance and showed potential applications in dental material.

Highlights

1. In-situ mullite toughened 3Y-TZP composite ceramics has been prepared by gel-casting, and the biotoxicity of mullite/3Y-TZP composites has been systematic studied, providing a precondition for its biomedical applications.
2. It reveals the bio-tribological behaviour and wear mechanism of mullite/3Y-TZP composites sliding against tooth enamel in artificial saliva environment, providing a theoretical basis for its practical dental applications.

1. Introduction

Advanced biomaterials made of metals and ceramics have received extensive attention and developed rapidly over the last few decades with the improvement of medical level and the development of materials [1-5]. It is well known that biomaterials, especially dental and bone repair ceramic materials, must have the characteristics of good biocompatibility, chemical stability and mechanical properties [6, 7]. Metal alloys, such as titanium alloys, are generally considered to be bio-inert in human biological systems. However, those alloys lack the ability to induce bone reconstruction when used for oral and bone bonding materials, which limits their long-term stability in vivo. In addition, the frequent interaction between alloys and physiological environment will release metal ions, which will be harmful to the patients' health [8-11].

Zirconia (ZrO_2) ceramic, as one of the most important oxide ceramics, not only in possession of bio-safety (no cytotoxicity), but also can exist stably in the oral environment without releasing harmful impurities and degradation [12-16]. In comparison with alumina (Al_2O_3) ceramic, ZrO_2 ceramic has more excellent mechanical properties, which can meet the requirements of higher compressive strength and hardness of dental ceramics [17-21]. Moreover, previous studies have confirmed that ZrO_2 ceramic shows poor bacterial adhesion. Scarano et al [22]. found that the coverage degree of bacteria on ZrO_2 was 12.1% as compared to 19.3% on titanium. Rimondini et al [22]. also confirmed these results through in-

vivo studies, and their results indicated that Y-TZP accumulated fewer bacteria than that of titanium in the total number of bacteria. Quinn et al [23]. studied the effects of microstructure and chemical composition on the mechanical properties of dental ceramics, and also believed that ZrO_2 ceramic had better mechanical properties than that of dental ceramics.

Despite ZrO_2 ceramic has high hardness and strength as well as good biocompatibility, the inherent brittleness limits its application. Mullite/3Y-TZP, as one of the ZrO_2 composite ceramics, not only improves the flexural strength and fracture toughness of pure ZrO_2 ceramic without introducing toxic composition, but also retains high hardness, which has been confirmed in our previous research [24, 25]. Nevertheless, in order to determine whether it is a better candidate for dental materials than pure ZrO_2 ceramic, further research is needed on the biotoxicity and tribological properties of mullite/3Y-TZP, which will play an important role in the service life and failure behavior of this material when used as a kind of dental ceramic.

Gergo Mitov et al [26]. used natural enamel to slide against Y-TZP ceramic treated in four different methods, and found that there was no significant linear correlation between the ceramic surface roughness and abrasive wear. Wang et al [27]. studied the wear behaviour of three dental ceramics (smooth and rough zirconia ceramics, glass ceramic, silicate-based veneer porcelain) sliding against tooth enamel with gold-palladium alloy and nickel-chromium alloy as control groups.The frictional coefficient of enamel sliding against polished zirconia or porcelain was between that of metal and glass-ceramic. Enamel showed abrasive wear when sliding against rough zirconia or glass ceramic. While fatigue wear was found on the worn surfaces of enamel when sliding against polished zirconia or nickel-chromium alloy, which showed that the friction and wear performance of zirconia can be improved significantly by proper surface polishing. Therefore, as a dental material, the study of its oral tribological behavior is very important.

In the previous study, high-performance mullite/3Y-TZP has been prepared by gel-casting combined with pressureless sintering. Based on the comprehensive analysis of the mechanical properties and microstructure of this ceramic, its biological toxicity will be confirmed by in vitro cytotoxicity tests including extract and direct contact methods in this study. These methods can be standardized to yield the repeatable results as well as efficiently performed at a relatively low cost [28, 29]. Moreover, the tribological properties of mullite/3Y-TZP will be deeply analyzed in terms of biology, including the study of wear behavior of the tooth enamel sliding against mullite/3Y-TZP in artificial saliva environment, and revealing their wear mechanism and wear resistance.

2. Experimental Procedures

2.1 Sample preparation

In this study, four human molars without obvious wear scar were derived from 18-year-old females, and stored in physiological saline for sample preparation after being removed from the body. Each tooth was

polished on carborundum sandpaper from 400 to 2000 mesh in water, and then polished by a polishing cloth. Finally, those teeth were cold-set by resin to obtain columnar pins with the size of φ10mm×15mm, and the enamel surface was exposed.

Commercially available ZrO_2 powders (AR grade, Shanghai Chemical Regent Co., China), SiO_2 powders (AR grade, Shanghai Chemical Regent Co., China) and Al_2O_3 powders (Sinopharm Chemical Reagent Co., Ltd., China) were used as raw materials. Y_2O_3 powders (Changsha Deli Rare Earth Chemical Co., Ltd. China) were used as sintering aids. Using gel-casting method (AM-MBAM system) combined with pressureless sintering to prepare rectangular mullite/3Y-TZP with the dimensions of 25mm×25mm×15mm. More details about this experimental process and raw materials used in this study were described in the Ref. 26. The polishing steps of these samples were similar to those for the teeth.

2.2 Characterization methods

The optical density (OD) of the medium in porous plate was measured by an absorbance microplate reader (ELx 800, USA). The morphologies of cells cultured with extract and direct contact methods were observed by inverted microscopy. Scanning electron microscope (SEM, JSM-6390, JEOL, Tokyo, Japan) was used to observe the surface morphologies of mullite/3Y-TZP and the tooth enamel before and after friction as well as wear debris. Using raman spectrum to analyze elemental composition and chemical bond information of mullite/3Y-TZP before and after friction tests. X-ray diffraction (XRD, Cu Ka radiation, D/max-2550–18kW, Rigaku, Japan) from 15° to 70° at 40kV with a scanning speed of 8°/min, coupled with energy dispersive X-ray spectroscopy (EDS) were used to analyze elemental composition and phase of mullite/3Y-TZP before and after friction as well as wear debris. The elemental distribution of the wear surface of mullite/3Y-TZP after friction was analyzed by electron probe microanalysis (EPMA). Using atomic force microscopy (AFM) and laser scanning confocal microscope (LSM700, Zeiss, Germany) to measure surface roughness (Ra) of the polished teeth and mullite/3Y-TZP as well as undulating state of the wear surface. An ultra depth of field three-dimensional microscopy system (VHX-500, Keyence, Japan) combine with LSM were used to characterize 3D morphologies of wear surface to determine the width and depth of the wear track.

2.3 Cytotoxicity tests

In vitro cytotoxicity assays were carried out on mullite/3Y-TZP according to ISO10993-5 using both extract and direct contact methods [30, 31]. The extract assays used L929 mouse fibroblasts as test cells. Each sample was ground into a cube of 6×6×6mm, and then they were ultrasonically cleaned with alcohol and deionized water, and finally put them into an autoclave for disinfection (121℃, 30min). Pure 3Y-ZrO_2 ceramic and mullite ceramic were used as the experimental control group, while the negative and positive control groups were also set. The flow diagram of the extract method is shown in **Fig. 1**, and the specific steps are as follows:

(1) Three different groups of the samples after disinfection were placed in the complete medium for 24h respectively, in which the ratio of the sample surface area to the volume of the culture medium was 1 and

$3cm^2/mL$;

(2) After the cells resuscitated and adhered to the wall for growth, the original culture medium was removed and the sample extract was added. 6 holes were set for each concentration of each sample group, and then placing them in the CO_2 incubator to culture for 1, 3 and 5 days, respectively;

(3) The viability of cells was assessed by using the tetrazolium salt (MTT), and ELx 800 was used to detect the OD value of each hole [32]. Then, calculating the RGR value according to the OD (optical density) value, and determining the cytotoxicity of the samples by combining with the cell morphologies.

Direct contact assays were performed using L929 mouse fibroblast. A cell suspension with a concentration of 5×10^4 cells/ml was dropped into a petri dish containing the sample, and the ratio of the sample surface area to the volume of the culture medium was 1:1. After being cultured in a CO_2 incubator for 1, 3 and 5 days, using inverted microscopy to observe the cell morphologies and determine whether there were transparent areas around the samples.

2.4 Tribological tests

All tribological tests were carried out using pin-disc wear combined with the cyclic reciprocating friction method on the UMT-3 multifunctional friction and wear tester in artificial saliva conditions. The **device diagram** and schematic diagram of the tribological tests are shown in **Fig. 2**. The tests used the teeth as bolts, while polished mullite/3Y-TZP were used as counterparts. During the chewing process of human beings, the chewing force between the upper and lower teeth in the mouth ranges from 3 to 36N and the sliding distance between the bite contacted teeth is about 0.9-1.2 mm.[33-35]. Therefore, A normal force of 20 N, cyclic reciprocating displacement of 1mm, and frequency of 2 Hz were used in all tribological tests, as shown in Table 1. The contents of various components of artificial saliva used in this experiment are shown in the Table 2 [27, 36]. The experiment was repeated three times in each condition. After friction test, the teeth and counterparts were ultrasonically cleaned and dried, and the wear rate was replaced by mass loss.

3. Results And Discussion

3.1 Cytotoxicity

The results of the extract assays are shown in **Fig. 3** and **Fig. 4**. The data have been analysed by one-way ANOVA, and the minimum significant difference at $p<0.05$ has been calculated and displayed on the histograms. There were no significant differences between any extracts of samples groups and the negative control group except the mullite group. A significant decrease of OD value happened in the positive control group, indicating that the tests were valid and L929 mouse fibroblasts cells were susceptible to the degrees of cytotoxicity.

The OD values (490nm) of each set of samples are shown in **Fig. 3**. Low OD values of all experimental groups were found after the cells had been cultured by extracts for 1 day, which was mainly because the cells did not fully grow and divide, and the cell concentration was low. Three days later, the OD values increased significantly except for the pure mullite group with a concentration of $3cm^2/mL$ and the positive control group. After being incubated for five days, the OD values of each experimental group were almost twice that of the cells cultured for 1 day, and each of them was not lower than that of the negative control group except the pure mullite group and the positive control group.

Combined with the comparison between the RGR value (>100%) and the determination standard of cytotoxicity level, ZrO_2 ceramic and mullite/3Y-TZP had no cytotoxicity, and morphologies of the cells of these groups also confirmed this result, as shown in **Fig. 4(a-b)** [32]. Although the RGR value of mullite group 100%, the result of morphologies of the cells cultured by extract of mullite for 5 days indicated that mullite had no cytotoxicity or slight cytotoxicity compared with that of the positive and negative control groups, as shown in **Fig. 4(c-e)**.

No adverse reaction was observed in petri dishes by inverted microscopy in the direct contact experiments, and morphologies of the cells are shown in **Fig. 5**. As depicted in **Fig. 5(a-c)**, no abnormalities or dead cells and cell-free transparent areas were found around the samples. Density and morphologies of the cells of these sample groups were similar to those of the negative control group (**Fig. 5(d)**), while there were significant death cells in the positive control group (**Fig. 5(e)**). The results showed that those three kinds of samples were no-cytotoxicity, which was a further proof of the previous experimental results.

3.2 Microstructure characterization

Fig. 6 shows the microstructure of mullite/3Y-TZP, from which it can be seen that there are two obviously different phases in the sample. The preliminary experimental results proved that the black phase was mullite generated by the reaction of Al_2O_3 and SiO_2 in the sintering process and the gray area was ZrO_2 [24, 25]. In the ternary eutectic system of Y_2O_3-SiO_2-Al_2O_3 formed by Y_2O_3 with SiO_2 and Al_2O_3, local liquid phase appeared in the sample at high temperature, then the contact reaction and nucleation occurred between SiO_2 and Al_2O_3. After that, the core of mullite crystal grew into the columnar crystal through mutual diffusion, as shown in **Fig. 6(a)** [37-41]. The size of the columnar mullite was about 10μm, as shown in **Fig. 6(b)**, and there were ZrO_2 particles uniformly distributed in the interior of mullite, which can improve the strength of columnar mullite by the pinning effect. Meanwhile, columnar mullite will also significantly enhance and toughen the composite ceramic for this reason. In addition, previous studies have shown that Y_2O_3 can enter the crystal lattice of ZrO_2 to stabilize the tetragonal/cubic phase [25].

The surface morphologies of the tooth enamel before the friction test are shown in **Fig. 6(c-d)**. It retained complete character with no protrusions or microcracks on the surface, providing a reliable premise for subsequent friction experiments. EDS analysis indicated that the main components of the tooth enamel

surface were calcium and phosphorus, and the atomic ratio of the two elements was about 1.6:1, confirming that tooth enamel was indeed made of hydroxyapatite ($Ca_{10}(PO_4)_6(OH)_2$), as shown in **Fig. 6(d)**, which provided a theoretical basis for subsequent analysis of wear debris.

3.3 Wear behavior

3.3.1 Coefficient of friction (μ) and mass loss

The Ra and 3D topographies of the polished tooth enamel and mullite/3Y-TZP before the friction test are shown in **Fig. 7**. Their Ra values were 33.6nm and 148.22nm respectively, indicating that the surfaces of these two kinds of materials using for friction tests were smooth, which can significantly reduce the frictional resistance (F_x) and μ [42]. As is known to us, there should be an appropriate μ when the dental implant sliding against natural teeth, so as not to cause excessive wear on one side or affect the chewing of food. The results were obtained by repeating the friction experiments for three times, and one of them was shown in **Fig. 8**. It can be seen that after a brief run-in period, the μ finally stabilized at 0.464. This value was between the μ of glass ceramics and Au-Pd alloy when rubbing against tooth enamel, and it was also in the range of μ when natural teeth chewing food [34]. The reason for getting this result was that even though the surfaces of this couple were very smooth before the friction test, they would be destroyed after the initial contact under the action of applied load, resulting in unstable μ and F_x until a new wear surface was generated. In the process of stable friction, the existence of artificial saliva played an important role in lubrication and cooling, but also could wash away the debris generated during the friction process and clean the wear surface. Therefore, the μ and F_x were decreased and extremely stable, and they were the factors that determined the mass loss of the teeth and mullite/3Y-TZP [34, 42]. This frictional behavior indicated that there was a good match between the tooth enamel and mullite/3Y-TZP.

The mass loss of the teeth and mullite/3Y-TZP was very small, even though the former value was slightly higher than that of the later, both of them lost a few milligrams, only were 0.5±0.1mg and 0.3±0.1mg, indicating that the wear resistance of the friction couple was well in this environment. Stable friction process and low wear rate proved that mullite/3Y-TZP had application potential in the field of oral cavity.

Moreover, Lee et al [43]. found that ZrO_2 would undergo phase transition under the action of load during the friction process, and the low wear rate of mullite/3Y-TZP may partly attributed to transformation toughening induced by flash-temperature. In this study, the diffraction peaks of different ZrO_2 phases of mullite/3Y-TZP did not show significant changes before and after the friction test, as shown in the XRD patterns of **Fig. 9**. The diffraction peaks intensity of m-ZrO_2, t-ZrO_2 and c-ZrO_2 were almost unchanged, which may be caused by stress dispersion and cooling effects of artificial saliva. In addition, the internal structure of mullite/3Y-TZP did not change before and after the friction test, as shown in the Raman spectrum of **Fig. 10** (black and red curves). The intensity of the diffraction peak and Raman shift of m-ZrO_2 and t-ZrO_2 did not change significantly [44]. The -OH peak (3625cm^{-1}) was observed in the Raman spectrum of mullite/3Y-TZP after the friction test, and Lang et al. [45, 46] mentioned that Y_2O_3 could react with water to form α-$Y(OH)_3$ due to the action of water and pressure during the friction process.

However, compared with the polished sample whose -OH peak most likely generated during the pretreatment process before the friction test, no new -OH peak formed during the friction process, This hypothesis was demonstrated by immersing mullite/3Y-TZP in artificial saliva for 5 days and then performing a Raman test, and the spectrum was shown in the blue curve. No significant changes happened in the intensity and Raman shift of the -OH peak, which was similar to those of the previous two results. These results indicated that mullite/3Y-TZP had good stability during friction and artificial saliva environments.

3.3.2 Wear appearances

Different observation methods were selected based on the different characteristics of the wear surface. 3D morphologies of the wear surface of the tooth enamel were measured by LSM700, and they showed a flat wear surface with almost no grooves and undulations, which can be obtained from **Fig. 11(a)**. The surface roughness of the wear surface was measured to be only 4.166μm, even though it was not as smooth as that of the original surface of the tooth enamel, and the curve at the bottom of **Fig. 11(a)** also illustrated no significant fluctuation. This phenomenon may be caused by the formation of smooth film on the wear surface due to the deformation of the debris falling from the tooth enamel under action of the artificial saliva and load during the friction process, which indicated that no significant abrasive wear had occurred on the surface of enamel, providing a basis for the following wear mechanism. Mullite/3Y-TZP, as a counterpart, did not produce severe wear on its wear surface compared to enamel, as shown in **Fig. 11(b)**. The 3D morphologies measured by VHX-500 demonstrated that the worn area of mullite/3Y-TZP was very shallow, and the vertical height difference between the centre of the pit and the unworn surface was only 8.37μm, as shown by the curve below **Fig. 11(b)**. The reason for this result was mainly because the hardness and strength of mullite/3Y-TZP were higher than that of the enamel on the surface of the tooth enamel, so it was difficult to cause severe wear on the composite ceramic in artificial saliva environment. These indicated that the good mechanical properties and surface topographies of the enamel and mullite/3Y-TZP made them have good matching and wear resistance.

Fig. 12(a) represents the overall appearance of the wear surface of the enamel at low magnification, and it showed a flat surface without significant scratches, which was consistent with its 3D morphologies. **Fig. 12(b)** shows the morphology obtained by local magnification of **Fig. 12(a)**. It can be seen that a small amount of abrasive debris adhered to the flat surface and the analysis of EDS showed that they were calcium-phosphorus compounds (hydroxyapatite) derived from the surface of the enamel with a small amount of elements in mullite/3Y-TZP and artificial saliva, as shown in the upper right corner of **Fig. 12(b)**. **Fig. 12(c)** shows a portion of the edge of the worn region, and it was apparent that delamination of the layered debris had occurred in this region, and the size was about 25μm, while cracks presented around it, which was closely related to stress-induced fatigue fracture.

Fig. 12(d) represents the overall appearance of the wear surface of mullite/3Y-TZP at a low magnification, and only a very small amount of scratches presented on the flat surface. A small amount of abrasive debris adhered to the surface of the counterpart, and EDS analysis showed that their

compositions were the same as that of the debris on the enamel surface, as shown in **Fig. 12(e)**. Unlike the wear surface of the enamel, the surface of mullite/3Y-TZP did not exhibit large-scale peeling, even though some scratches and microcracks appeared, as shown in **Fig. 12(f)**, which was closely related to the mechanical properties of mullite/3Y-TZP. In addition, the pinning effect of mullite and good combination between the ZrO_2 particles reduced the likelihood of particle flaking.

In order to further analyze the element distribution of the wear surface of mullite/3Y-TZP, EPMA analysis was performed, as shown in **Fig. 13**, where Al and Si elements were not indicated. As shown in **Fig. 13(a-d)**, the internal components Zr and Y of mullite/3Y-TZP were detected, and it clearly proved that Y element distributed uniformly in ZrO_2, which played a role in stabilizing t-ZrO_2. In addition to the components of the ceramic matrix, there were also Ca and P elements on the wear surface, as shown in **Fig. 13(e-f)**, indicating that there was wear debris from the enamel presented on the wear surface, which can be found in the grooves in combination with **Fig. 13(a)**. The representative elements Na, Cl, etc. in artificial saliva also existed on the wear surface, and their distribution was consistent with that of Ca and P elements besides a small amount of them evenly distribute in other areas, which was mainly because of the adsorption of wear debris to artificial saliva. It was apparent that the filling of grooves and cavities with wear debris and artificial saliva can significantly lubricate the wear surface and reduce friction resistance.

3.3.3 Wear mechanism

The shape of the wear debris provides a reliable clue to the wear mechanism of the specimen. **Fig. 14** shows the morphologies of the wear debris obtained after the tooth enamel sliding against mullite/3Y-TZP under artificial saliva, from which abrasive grains and layered wear debris with different sizes can be seen. The size of abrasive grains was small with obvious aggregation and adhesion to each other; While the layered debris had two kinds of morphologies, which were large layered debris with a rough surface, as shown in **Fig. 14(a-b)**, and the layered debris having a smooth surface, as shown in **Fig. 14(c-d)**, respectively. On the surface of the first kind of lamellar debris, there were fine particles aggregating and obvious microcracks, which was caused by the aggregation of abrasive debris under the combined action of artificial saliva and load during the friction process, or directly from the lamellar shedding on the surface of the enamel. The second kind of lamellar debris had a clear outline with brittle fracture boundaries and microcracks, indicating that they were mainly exfoliated on the enamel surface, as shown in **Fig. 15(a-d)**. It can be seen that the mass ratio of three elements of calcium, phosphorus and oxygen in the wear debris was high, reaching 26%, 18% and 24% respectively, and they were distributed almost every debris combined with **Fig. 15(a)**. In addition, the surface of the wear debris was evenly distributed with a small amount of debris from the surface of the mullite/3Y-TZP and elements in the artificial saliva, as shown in **Fig. 15(e-i)**, which indicated that only slight wear occurred in mullite/3Y-TZP, thus it was difficult to find large pieces of ZrO_2 particles in the wear debris. The filling and lubrication of the wear surface by artificial saliva reduced the frictional resistance and wear rate, and result in the adhesion of elements, such as Na and K on the surface of the enamel and counterpart.

The morphologies of the wear debris combined with the wear surface of the tooth enamel indicated that it mainly experienced fatigue wear. Because the enamel located on the surface of the tooth was hard and brittle, repeated friction and load will cause stress concentration in the contact part, resulting in fatigue fracture [34]. Therefore, there were lamellar detachment areas and brittle fracture boundaries as well as microcracks on the wear surface of the tooth enamel, and many falling layered wear debris also appeared. In addition, the shape of the edge portion of the wear surface indicated that adhesive wear was locally occurred(**Fig.12(a)**), which was due to the film formed on the wear surface after the abrasive was wetted and pressed, and the film was peeled off due to repeated friction for a long time. Thereby, an adhesive wear zone was formed.

However, whether it was from the wear rate and wear surface morphologies of mullite/3Y-TZP or the elemental analysis of the wear debris, mild wear of mullite/3Y-TZP could be obtained. The uniform distribution of Zr, Al and Si elements in the wear debris indicated that mullite/3Y-TZP did have a slight particle flaking phenomenon and only occur mild abrasive wear, which was also consistent with a few scratches on its wear surface. The lubrication and cooling effects of the wear debris and artificial saliva which filled in the pits of the wear surfacec of mullite/3Y-TZP maintained the entire friction process at an extremely low wear rate during the repeated friction tests. Because the hardness of the enamel was lower than that of mullite/3Y-TZP and artificial saliva had lubrication and cooling effects, it was difficult to cause extensive fatigue wear on the composite ceramic. In addition, almost no phase transformation of ZrO_2 was obtained by the previous XRD analysis during the friction process, and Raman analysis found no significant reaction between Y_2O_3 with water, indicating that the internal structure of mullite/3Y-TZP was retained, which played an important role in retaining high mechanical properties. This phenomenon showed that mullite/3Y-TZP had good stability and wear resistance in the human oral environment.

4. Conclusion

The cytotoxicity of mullite/3Y-TZP has been preliminarily studied based on its dental application, and the tribological properties of the tooth enamel sliding against mullite/3Y-TZP in artificial saliva environment have been deeply analyzed with mullite/3Y-TZP as the counterpart. The main conclusions are as follows:

1. The cytotoxicity of mullite/3Y-TZP was tested by both extract and direct contact methods. The results indicated that mullite/3Y-TZP did not show acute cytotoxicity like ZrO_2 ceramic, even though the second phase of mullite was introduced.
2. In artificial saliva environment, the friction process between the tooth enamel and mullite/3Y-TZP was extremely stable with the μ of 0.464. The wear rate of the two materials was slight due to the lubrication and cooling effects of artificial saliva. These tribological properties showed that the friction pairs matched well.
3. No significant phase transitions happened to mullite/3Y-TZP during the friction test. The tooth enamel mainly suffered from fatigue wear accompanied by slight adhesive wear due to the filling of

artificial saliva and wear debris. While mullite/3Y-TZP only showed slight abrasive wear in this condition. These results indicated that mullite/3Y-TZP had good stability and wear resistance.

Declarations

Acknowledge

The authors gratefully acknowledge the financial supports from the National Natural Science Foundation of China (Grant No. 51575536) and State Key Laboratory of Powder Metallurgy.

References

1. Nath S, Basu B. *Materials for orthopedic applications*. *Adv Biomater* 2010: *53–100*
2. Fu SY, Zhu M, Zhu Y (2019) Organosilicon polymer-derived ceramics: An overview. J Adv Ceram 8:457–478
3. Matasa CG (2000) Trends in orthodontic biomaterials: metals and ceramics. Orthod Fr 71:335
4. Affatato S, Ruggiero A, Merola M. Advanced biomaterials in hip joint arthroplasty. A review on polymer and ceramics composites as alternative bearings. Compos Part B Eng 2015, 83: 276–283
5. Afzal A. *Implantable ZrO_2 bioceramics for bone repair and replacement: A chronological review*. *Mater Express* 2014, *4*: *1–12*
6. Anselme K (2000) Osteoblast adhesion on biomaterials. Biomater 21:667–681
7. Sivakumar R (1999) On the relevance and requirements of biomaterials. B Mater Sci 22:647–655
8. Bandyopadhyay A, Bose S, Roy M et al (2012) MgO-doped tantalum coating on Ti: Microstructural study and biocompatibility evaluation. Acs Appl Mater Inter 4:577–580
9. Scarano A, Piattelli M, Caputi S et al (2004) Bacterial adhesion on commercially pure titanium and zirconium oxide disks: an in vivo human study. J Periodonto 75:292–296
10. Khan MA, Williams R L, Williams DF. In-vitro corrosion and wear of titanium alloys in the biological environment. Biomater 1996, 17: 2117
11. Hodgson AWE, Mueller Y, Forster D et al Electrochemical characterisation of passive films on Ti alloys under simulated biological conditions. Electrochim Acta 2003, 47: 1913–1923
12. Piconi C, Maccauro G. Zirconia as a ceramic biomaterial. Biomater 1999, 20: 1
13. Afzal A (2014) Implantable zirconia bioceramics for bone repair and replacement: A chronological review. Mater Express 4(12):1–12
14. Christel P, Meunier A, Heller M et al Mechanical properties and short-term in vivo evaluation of yttria-oxide-partially-stabilized zirconia. J Biomed Mater Res 1989, 2: 45–61
15. Josset Y, Oum'Hamed Z, Zarrinpour A et al In vitro reactions of human osteoblasts in culture with zirconia and alumina ceramics. J Biomed Mater Res 2015, 47: 481–493

16. Carlo FD, Prosper L, Ripari F et al Bone response to zirconia ceramic implants; an experimental study in rabbit. Key Eng Mater 2001, 192–195: 403–408
17. Teng X, Liu H, Huang C. *Effect of Al_2O_3, particle size on the mechanical properties of alumina-based ceramics*. Mater Sci Eng A 2007, 452: 545–551
18. Vasylkiv O, Sakka Y, Skorokhod VV. Low-temperature processing and mechanical properties of zirconia and zirconia-alumina nanoceramics. J Am Ceram Soc 2003, 86: 6
19. Zhang Y (2013) Mechanical properties of zirconia composite ceramics. Ceram Int 39:7595–7603, Vaßen, Robert, Mack D E, et al.
20. Pilathadka S, Vahalová D, Vosáhlo T. The Zirconia: a new dental ceramic material. An overview. Prague Med Rep 2007. 108: 5–12
21. Vagkopoulou T, Koutayas SO, Koidis P et al Zirconia in dentistry: Part 1. Discovering the nature of an upcoming bioceramic. Eur J Esthet Dent 2009, 4: 130–151
22. Rimondini L, Cerroni L, Carrassi A et al Bacterial colonization of zirconia ceramic surfaces: An in vitro and in vivo study. Int J Oral Maxillofac Implants 2002, 17: 793–798
23. Quinn JB, Sundar V, Lloyd IK. Influence of microstructure and chemistry on the fracture toughness of dental ceramics. Dent Mater 2003, 19: 603–611
24. Huang YQ, Li Z, Liu PF et al Effects of the content of in-situ grown mullite on the microstructure and mechanical properties of 3Y-TZP ceramics fabricated by gel-casting. Ceram Int 2018, 44: 21882–21892
25. Liu PF, Li Z, Xiao P et al Microstructure and mechanical properties of in-situ grown mullite toughened 3Y-TZP zirconia ceramic fabricated by gel-casting. Ceram Int 2018, 44: 1394–1403
26. Gergo M, Siegward D, Stephanie W. Wear behavior of dental Y-TZP ceramic against natural enamel after different finishing procedures. Dent Mater 2012, 28: 909–918
27. Wang L, Liu Y H, Si WJ et al Friction and wear behaviors of dental ceramics against natural tooth enamel. J Eur Ceram Soc 2012, 32: 2599–2606
28. Eldeniz AU, Mustafa K, Orstavik D et al Cytotoxicity of new resin-, calcium hydroxide- and silicon-based root sealers on fibroblasts derived from human gingiva and L929 cell lines. Int Endod J 2010, 40: 329–337
29. Williams DF (2008) On the mechanisms of biocompatibility. Biomater 29:2941–2953
30. *ISO 10993-5. Biological evaluation of medical devices-Part 5: tests for in vitro cytotoxicity. International Organization for Standardization.*
31. Mossman T (1983) Rapid colorimetric assay for cellular growth and survival: application to proliferation and cytotoxicity assays. J Immunol Methods 65:55–63
32. Ciapetti G, Cenni E, Pratelli L et al In vitro evaluation of cell/biomaterial interaction by MTT assay. Biomater 1993, 14: 359–364
33. Zhou ZR, Yu H Y, Zheng J et al *Effect of the Oral Environment on the Tribological Behavior of Human Teeth. Dent Biotribol 2013: 75–115*

34. Riro B (2001) Frontal-plane lateral border movements and chewing cycle characteristics. J Oral Rehabil 28:930–936
35. Embong A, Glyn-Jones J, Harrison A. The wear effects of selected composites on restorative materials and enamel. Dent Mater 1987, 3: 236–240
36. Holland RI (1980) Galvanic currents between gold and amalgam. Scand J Dent Res 88:269–272
37. Zhu WW, Jiang H F, Zhang H. *Effect of TiO_2 and CaF_2 on the crystallization behavior of Y_2O_3-Al_2O_3-SiO_2 glass ceramics*. Ceram Int 2018, 44: 6653–6658
38. Mecartney ML (1987) Influence of an amorphous second phase on the properties of yttria-stabilized tetragonal zirconia polycrystals (Y-TZP). J Am Ceram Soc 70:54–58
39. Qin H, Huang X. Microstructure and bending strength of 3Y-TZP/12Ce-TZP ceramics fabricated by liquid-phase sintering at low temperature. J Am Ceram Soc 2000, 83: 2881–2883
40. Jr TJM, Laughner J W. Microstructures of mullite sintered from seeded sol-gels. J Am Ceram Soc 1989, 72: 508–509
41. Huang T, Rahaman M N, Mah TI et al *Effect of SiO_2 and Y_2O_3 additives on the anisotropic grain growth of dense mullite*. J Mater Res 2000, 15: 718–726
42. Buciumeanu M, Queiroz J R C, Martinelli AE et al The effect of surface treatment on the friction and wear behavior of dental Y-TZP ceramic against human enamel. Tribol Int 2017, 116: 192–198
43. Lee SW, Hsu S M, Shen MC. Ceramic wear maps: Zirconia. J Am Ceram Soc 2010, 76: 1937–1947
44. Tang XL, Zheng X H. *Raman Scattering and t-Phase Lattice Vibration of 3% (mole fraction) Y_2O_3-ZrO_2*. J Mater Sci Technol 2004, 20: 485–489
45. Monosmith WB, Walrafen G E. Temperature dependence of the Raman OH-stretching overtone from liquid water. J Chem Phys 1984, 81: 669
46. Lange FF, Dunlop G L, Davis BI. *Degradation During Aging of Transformation-Toughened ZrO_2-Y_2O_3 Materials at 250 °C*. J Am Ceram Soc 2010, 69: 237–240

Tables

Table 1. Experimental parameters and results of the friction test

Experimental parameters					Experimental conditions	Experimental results	
Specimen :Counterpart	Speed	Load	Time	Displacement	Environment	Average μ	Mass loss
	r/min	N	min	mm			mg
Tooth :Mullite/3Y-TZP	180	30	60	1	Artificial saliva	0.464	0.5±0.1
							0.3±0.1

Table 2. Composition of artificial saliva

NaCl	KCl	$CaCl_2 \cdot 2H_2O$	$NaH_2PO_4 \cdot 2H_2O$	$Na_2S \cdot 9H_2O$	Urea	Distilled water
0.4g	0.4g	0.795g	0.78g	0.005g	1g	1000mL

Figures

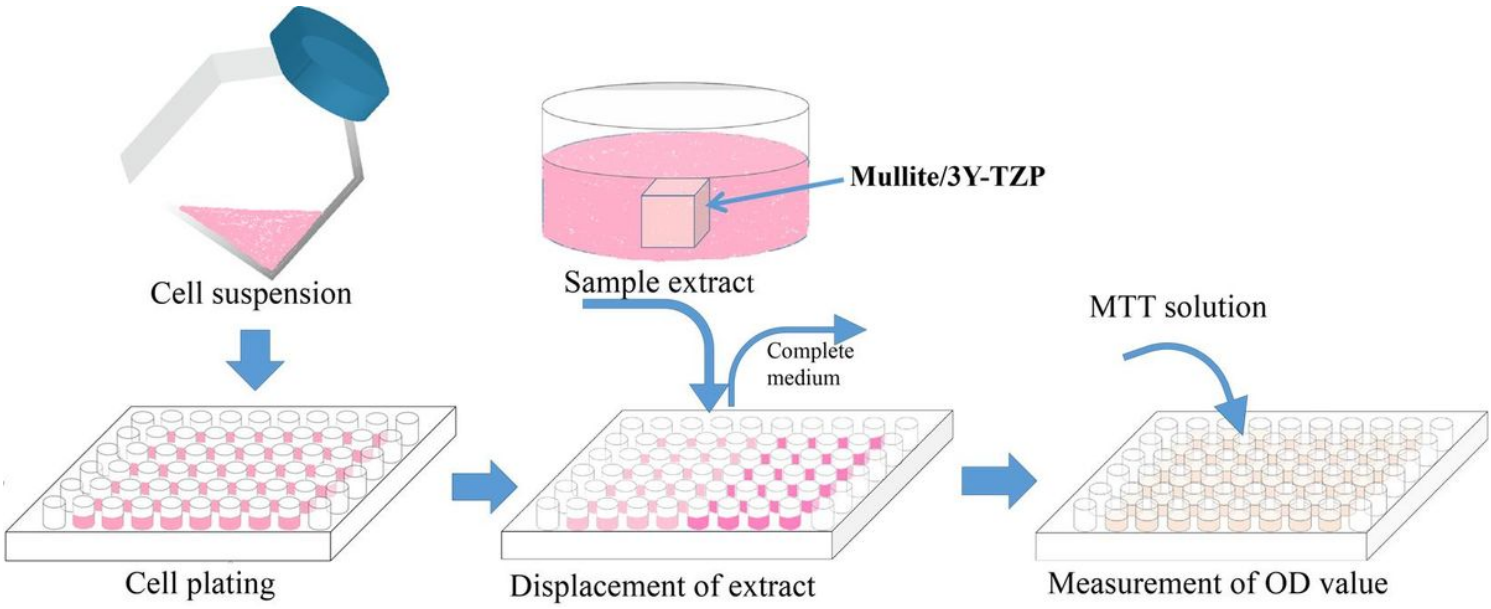

Figure 1

Flow diagram of the extract method.

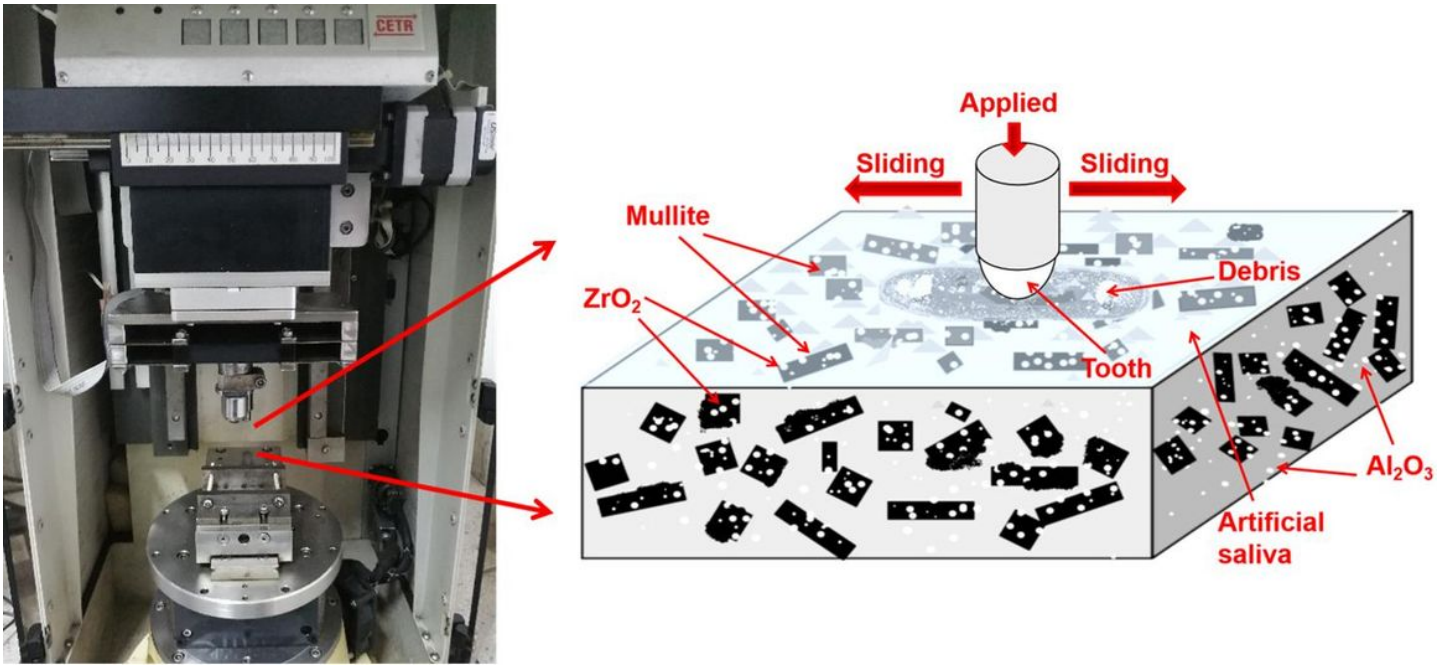

Figure 2

Device diagram and schematic diagram of the friction test.

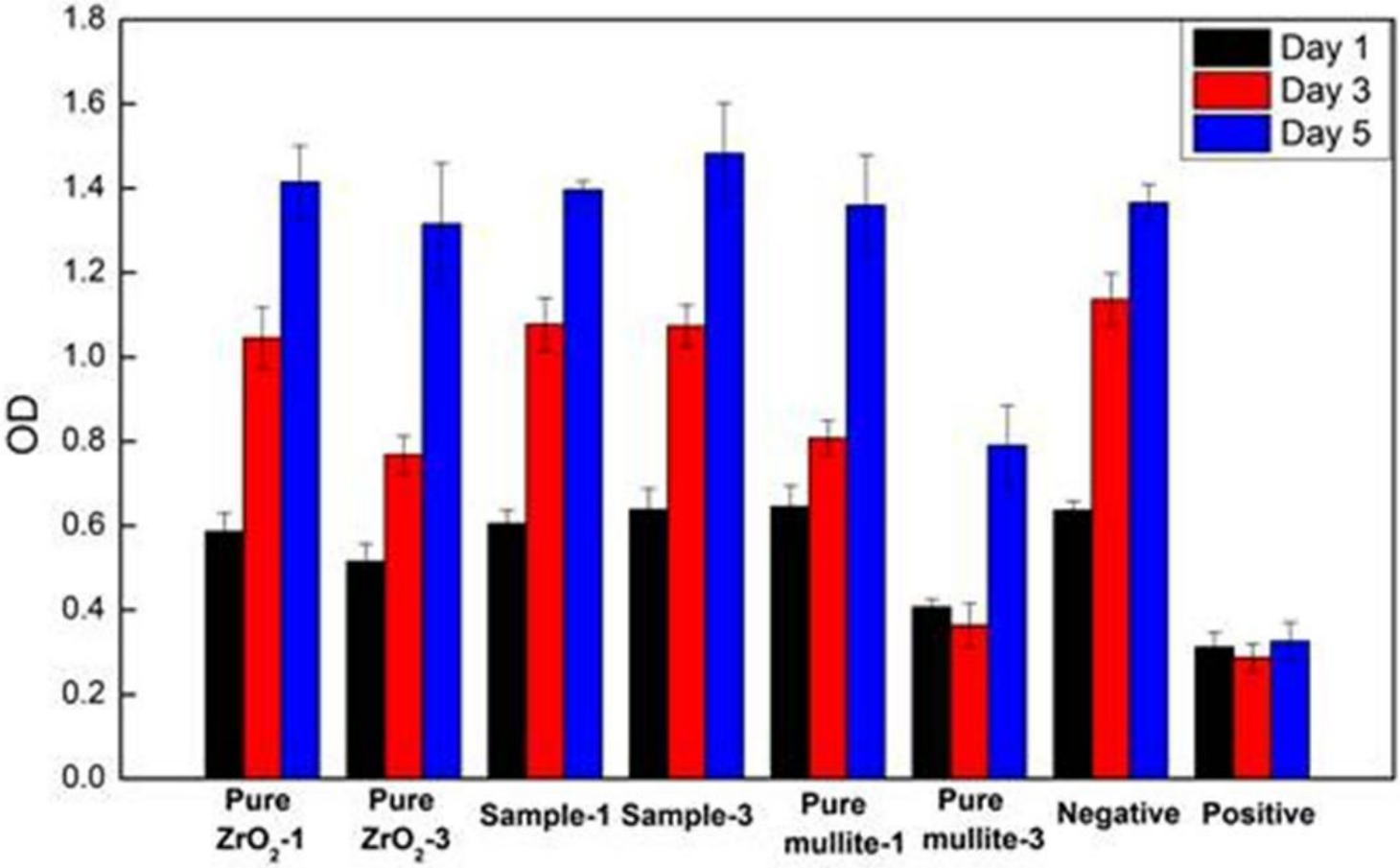

Figure 3

Cytotoxicity assessment of each group of sample using L929 mouse fibroblast.

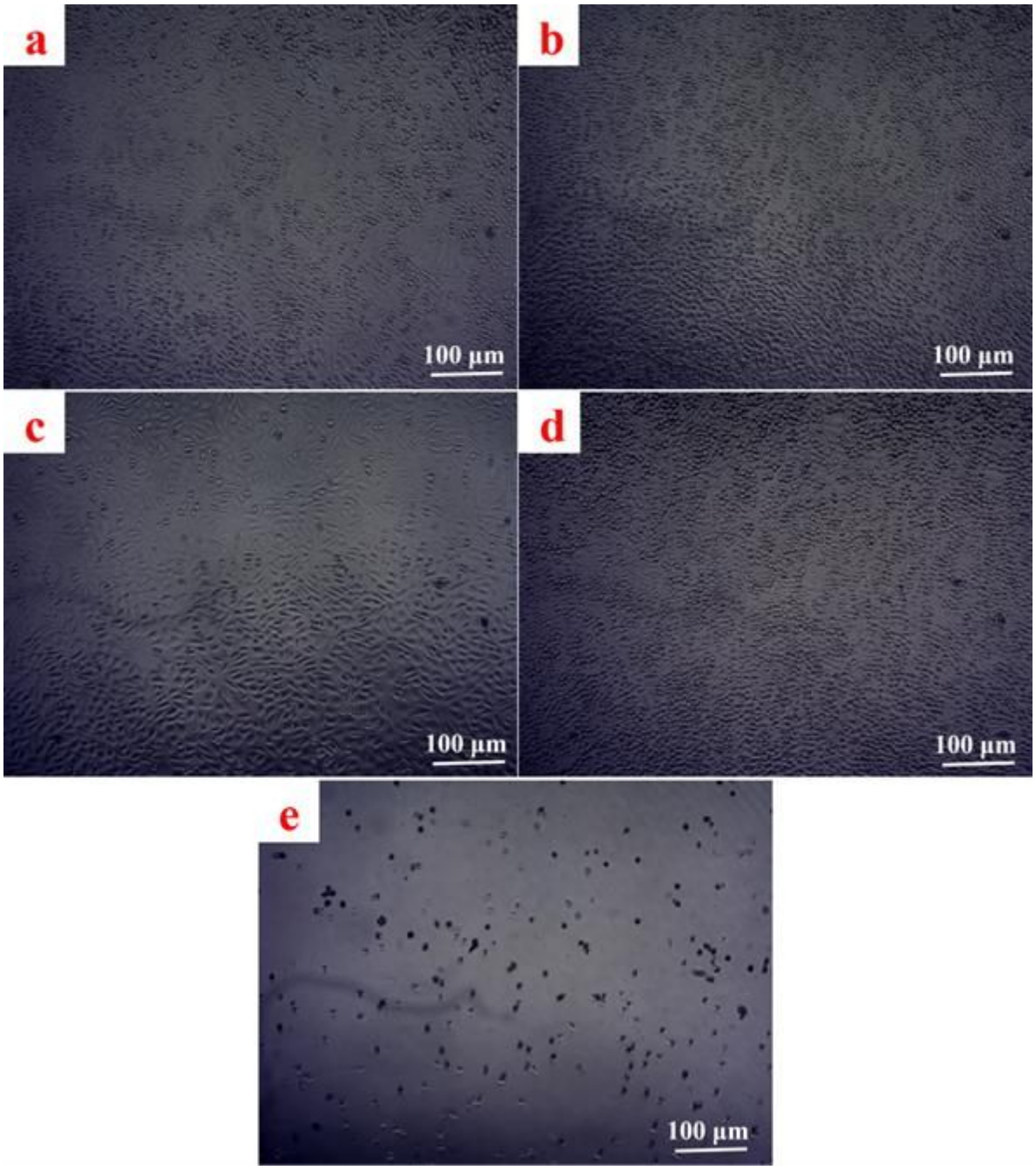

Figure 4

Morphologies of cells cultured at 3cm2/mL for 5 days in different groups. (a-c): extract of mullite/3Y-TZP, 3Y-TZP and mullite; (d-e): Negative and positive control groups.

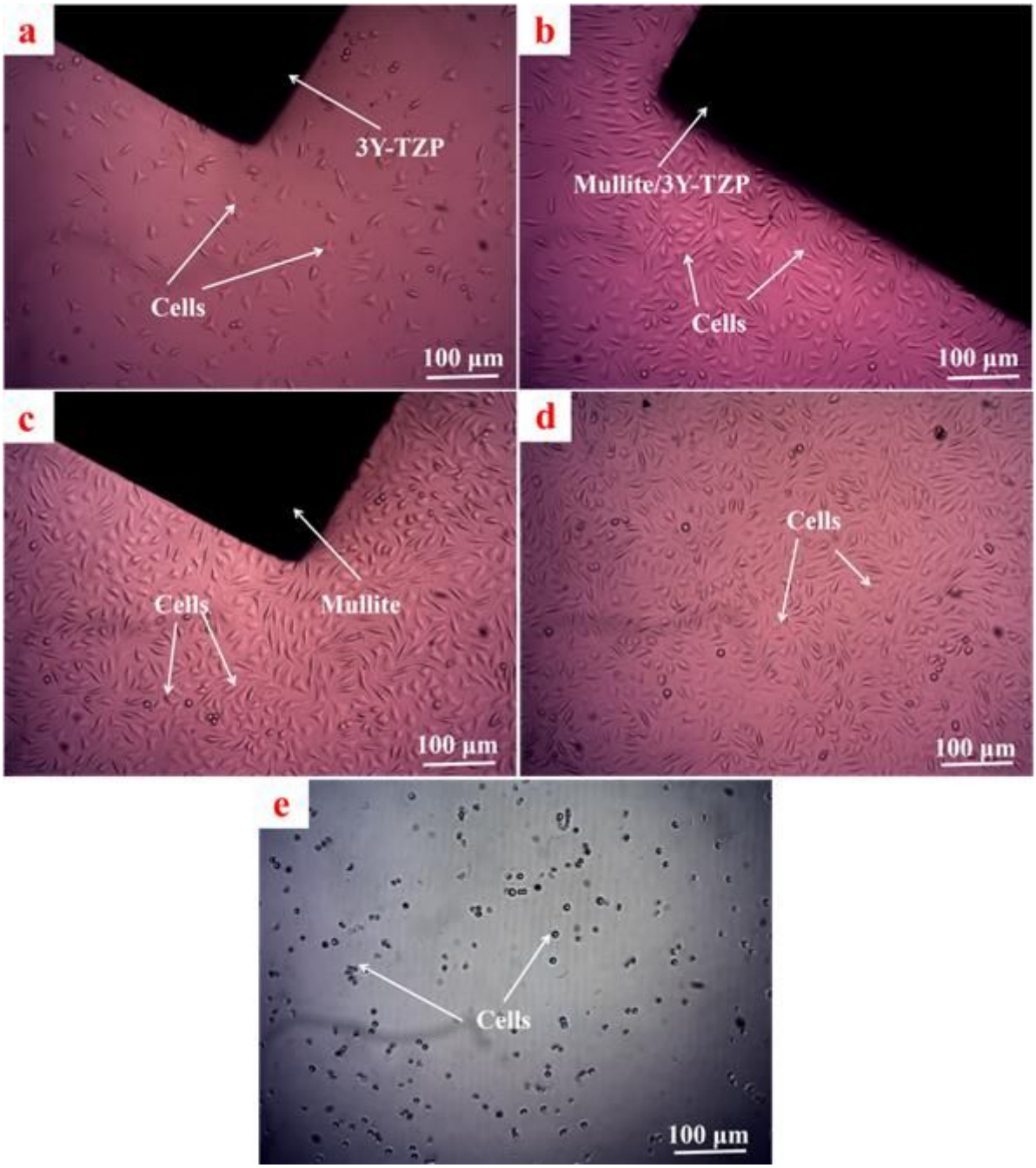

Figure 5

Morphologies of cells cultured for 5 days by the direct contact method. (a-c): The groups of mullite/3Y-TZP, 3Y-TZP and mullite; (d-e): Negative and positive control groups.

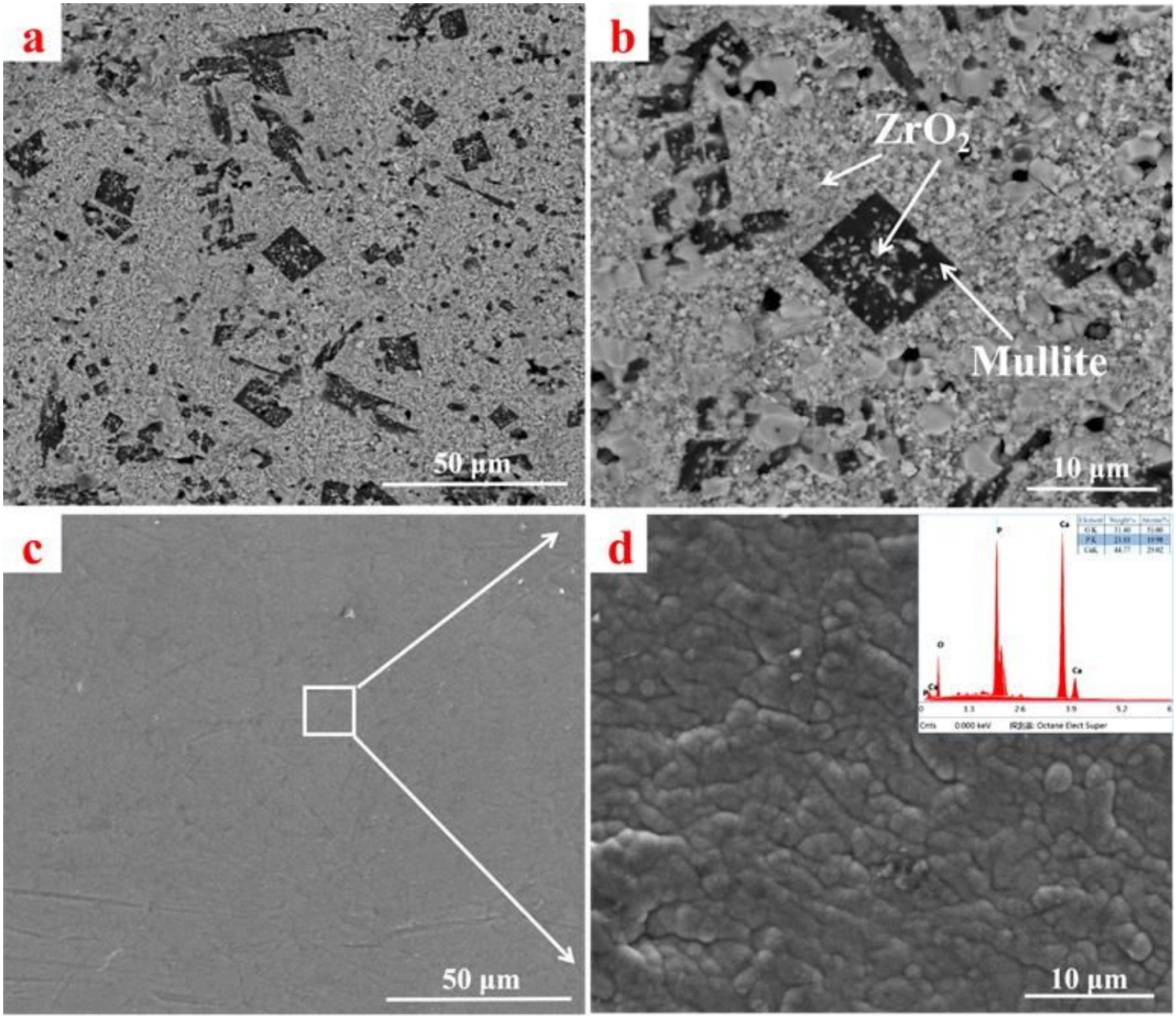

Figure 6

(a-b): SEM images of the surface of mullite/3Y-TZP; (c-d): SEM images and EDS of the surface of the tooth enamel.

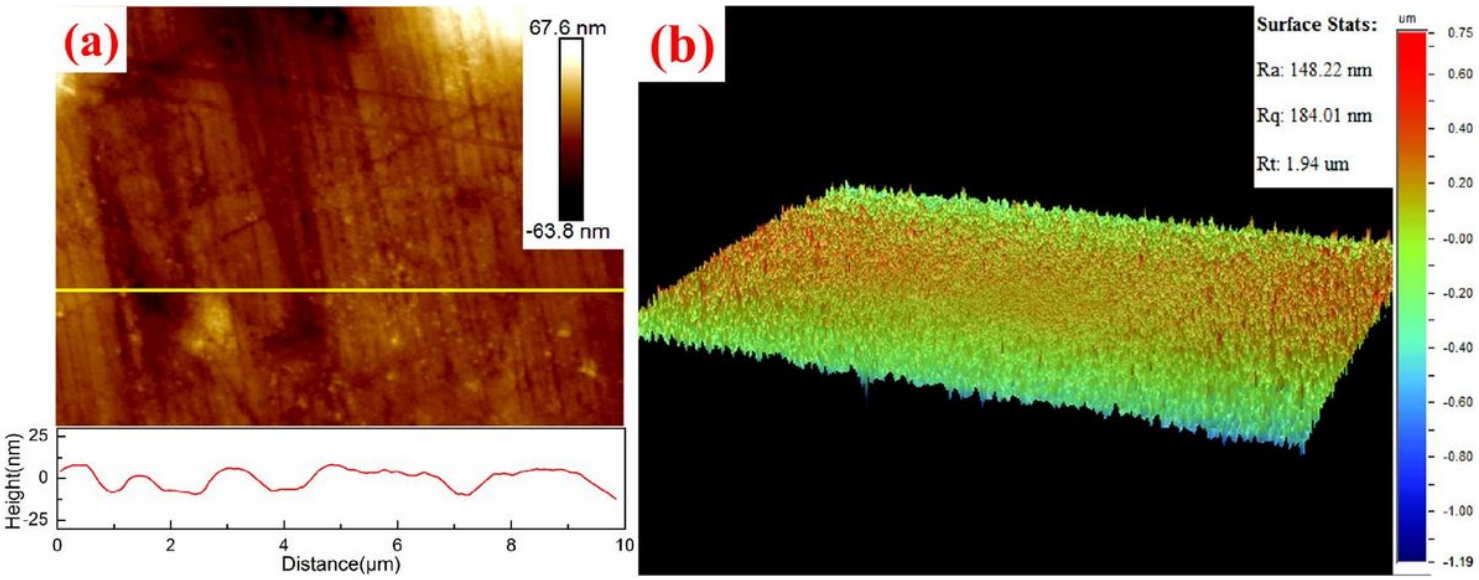

Figure 7

Surface roughness and 3D morphology before the friction test. (a): Polished teeth; (b): Mullite/ 3Y-TZP.

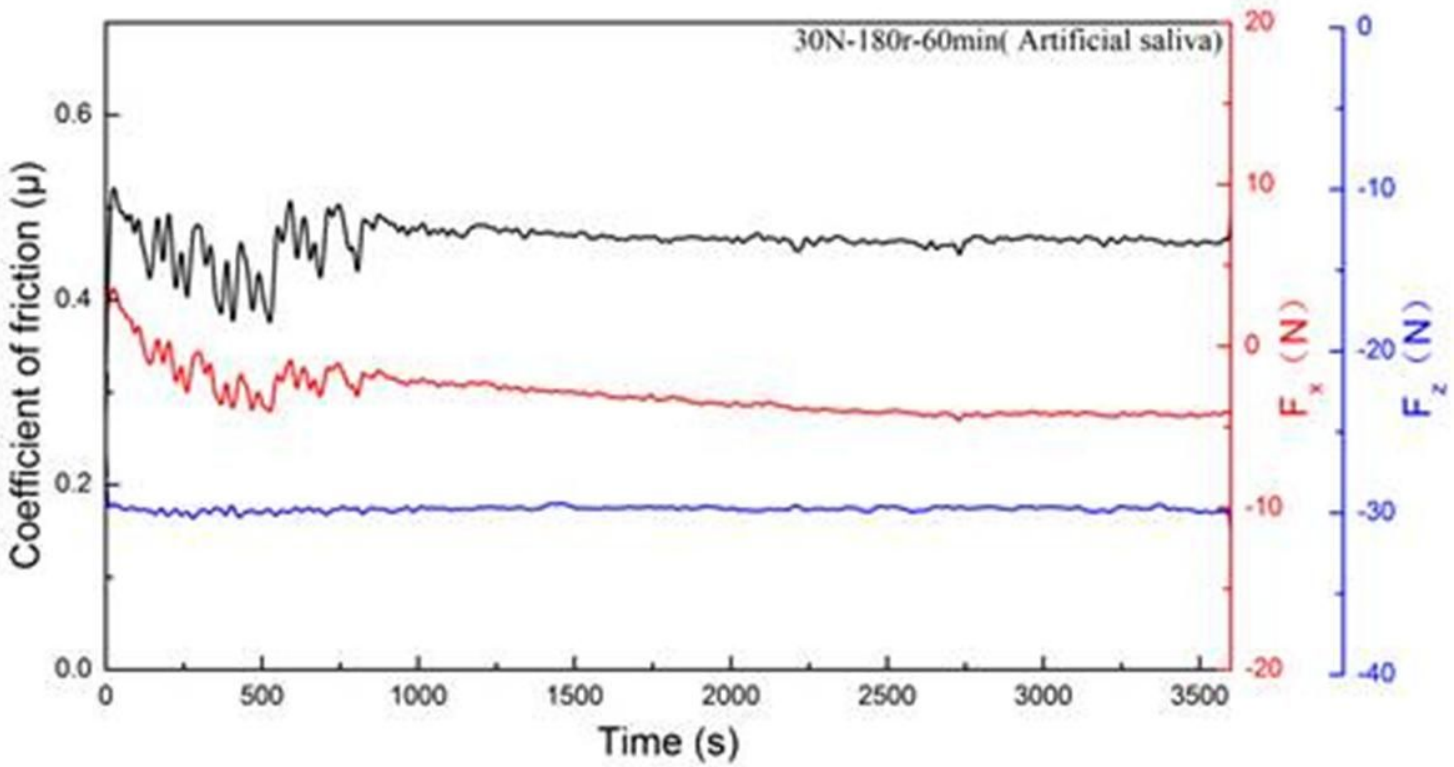

Figure 8

The curves of the coefficient of friction (μ), friction resistance (Fx) and applied load (Fz) during the friction test.

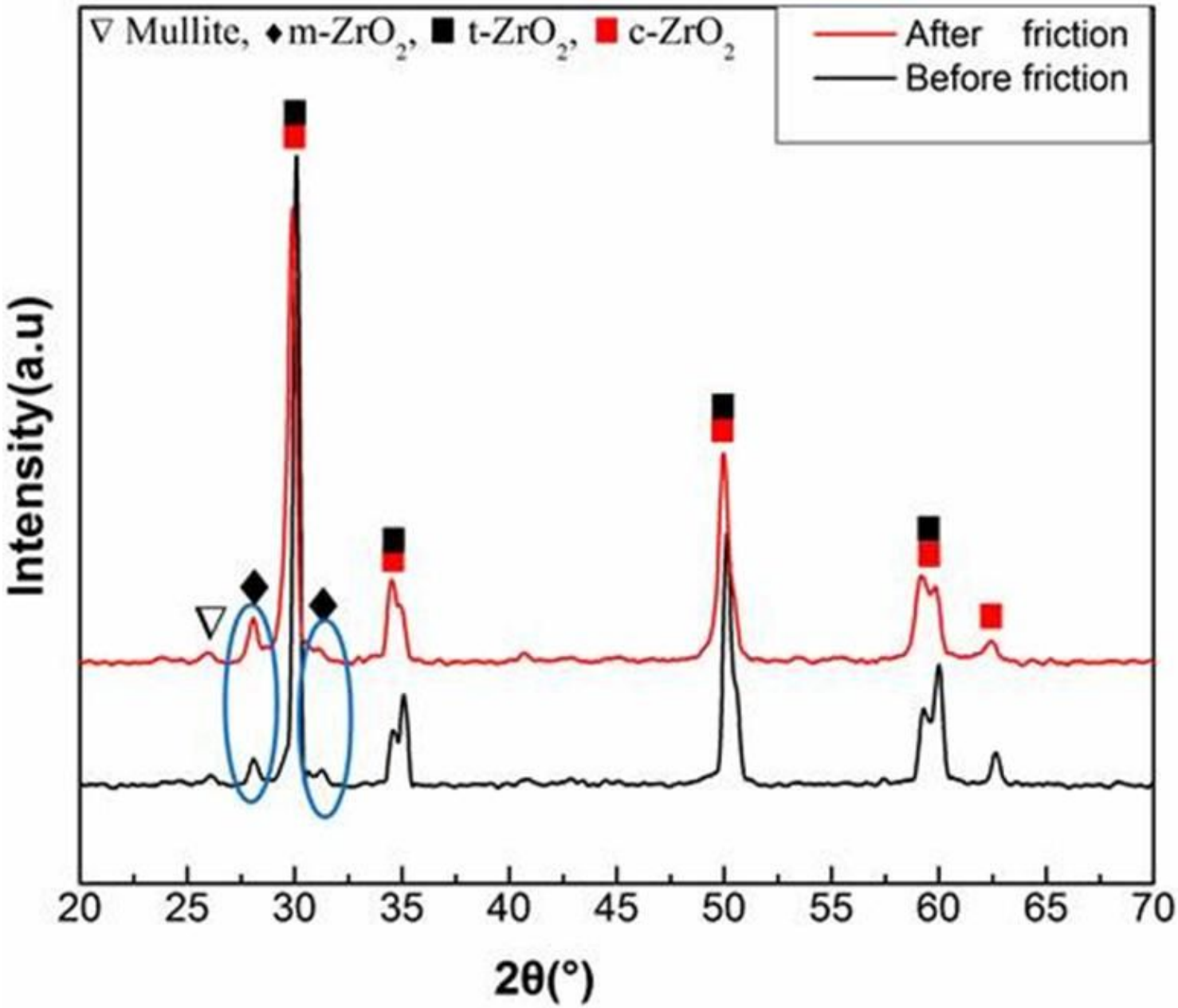

Figure 9

XRD patterns of mullite/3Y-TZP before and after the friction test.

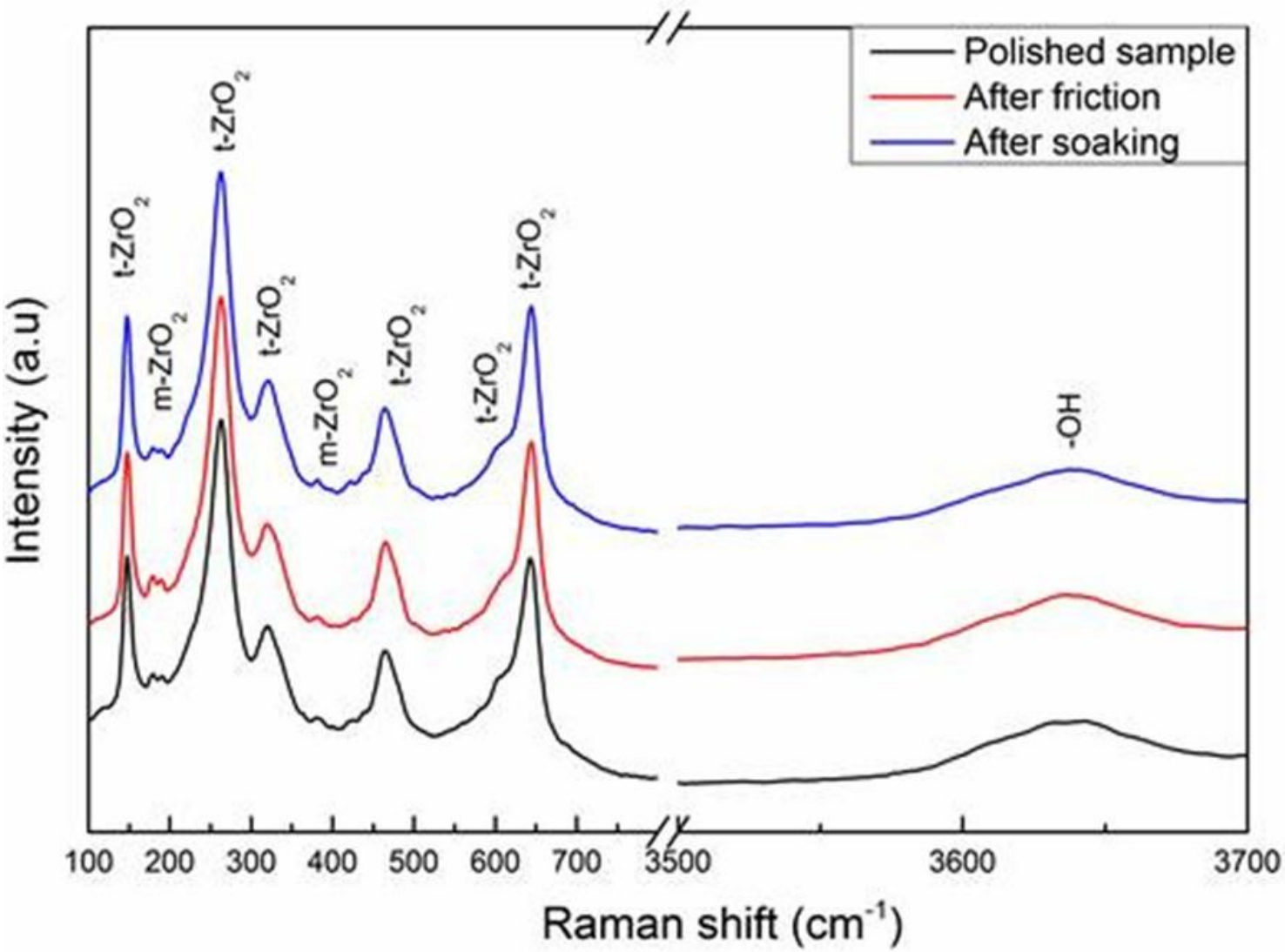

Figure 10

Raman spectrum of mullite/3Y-TZP with different methods of handling.

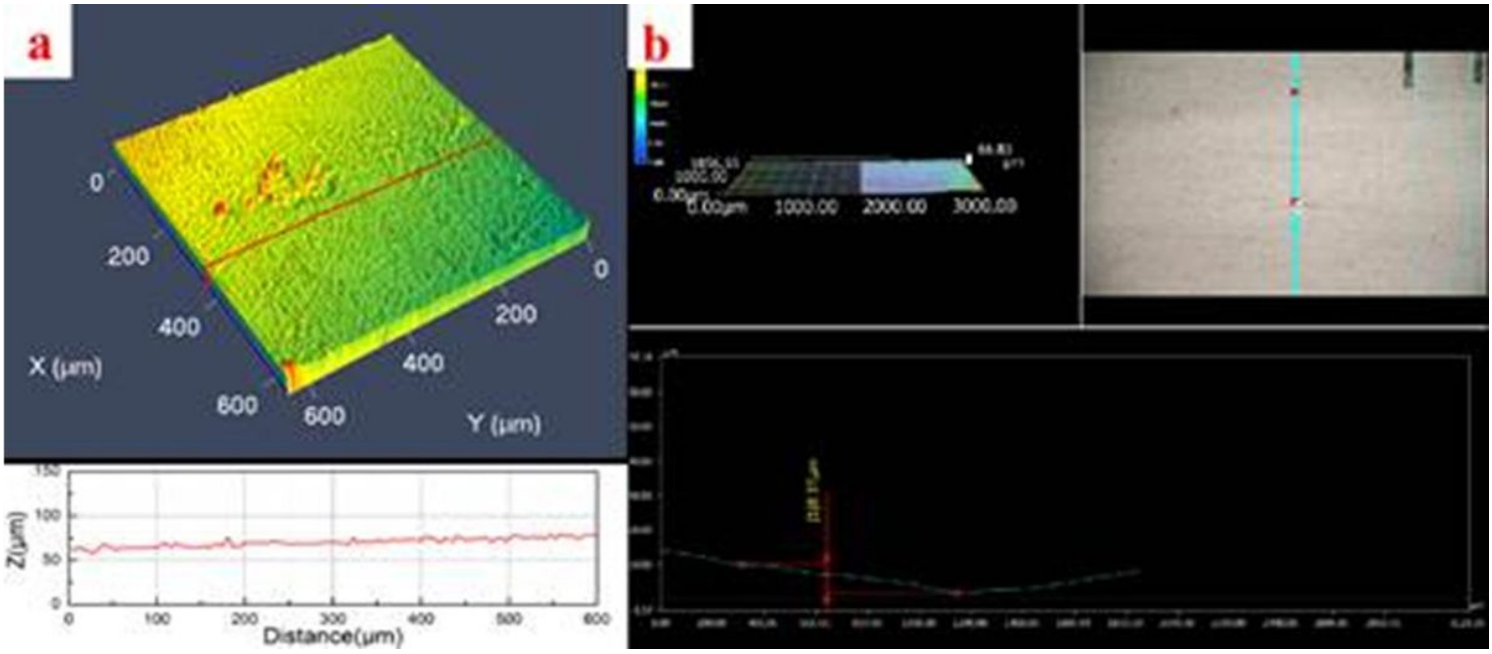

Figure 11

3D morphologies of the wear surface after friction test by different devices. (a): the enamel (LSM700); (b): Mullite/3Y-TZP (VHX-500).

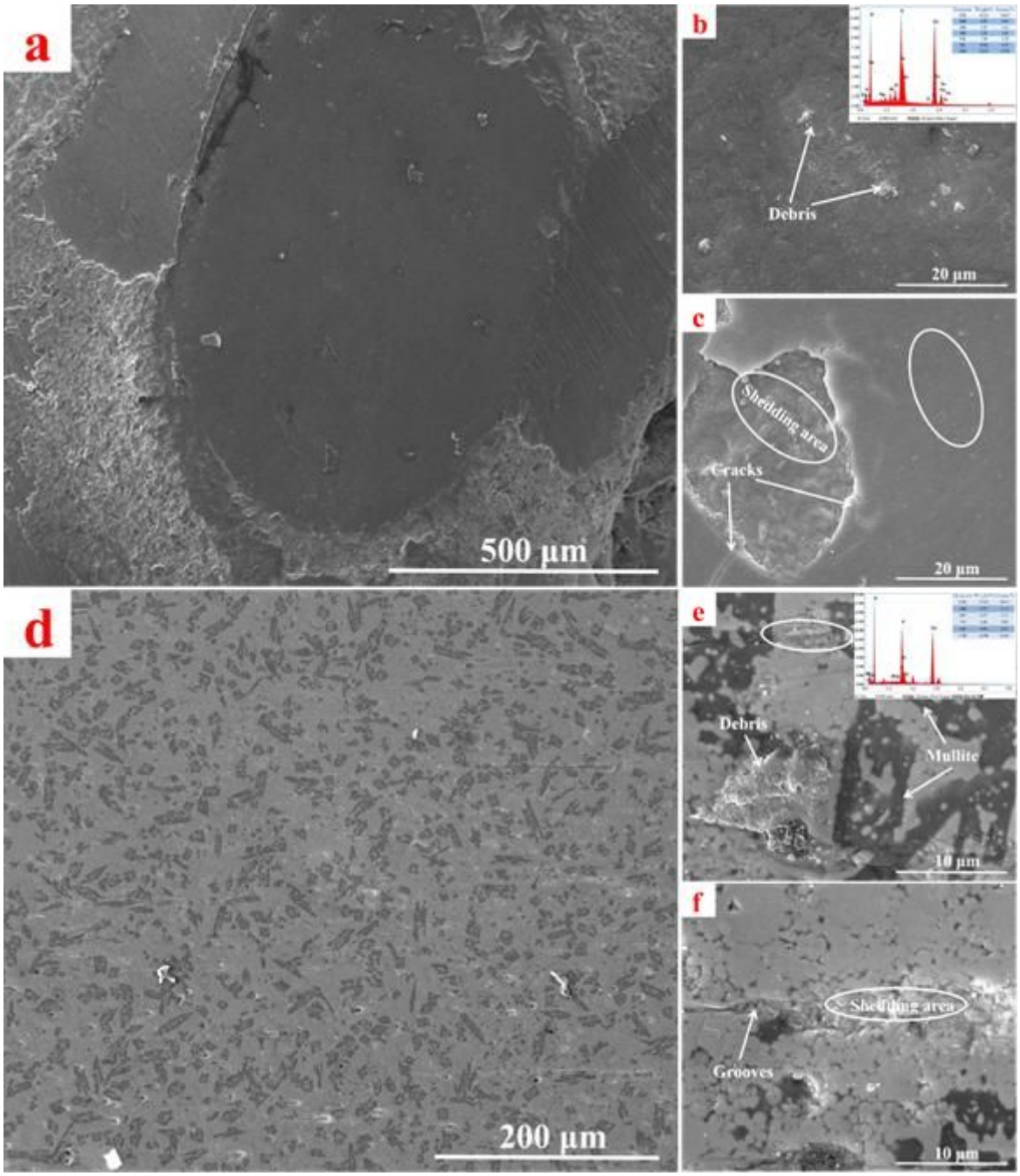

Figure 12

(a): Overall microscopic morphology of the wear surface of the enamel; (b): Wear debris and its energy spectrum; (c): The local magnification of (a). (d): Overall microscopic morphology of the wear surface of mullite/3Y-TZP; (e): Wear debris and its energy spectrum; (f): The local magnification of (a).

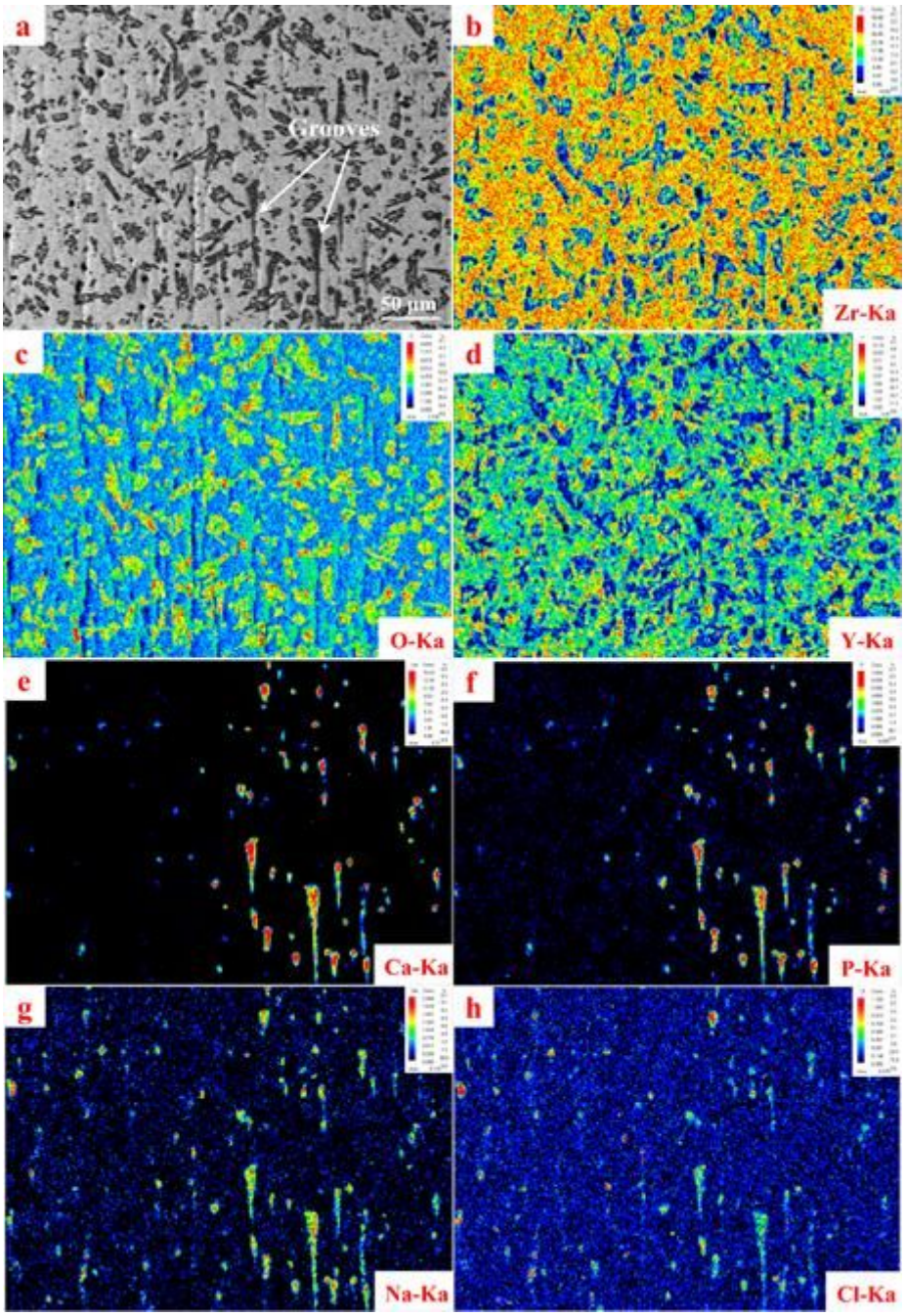

Figure 13

(a): Morphologies of the wear surface of mullite/3Y-TZP, (b-h): Distribution of various elements in this area.

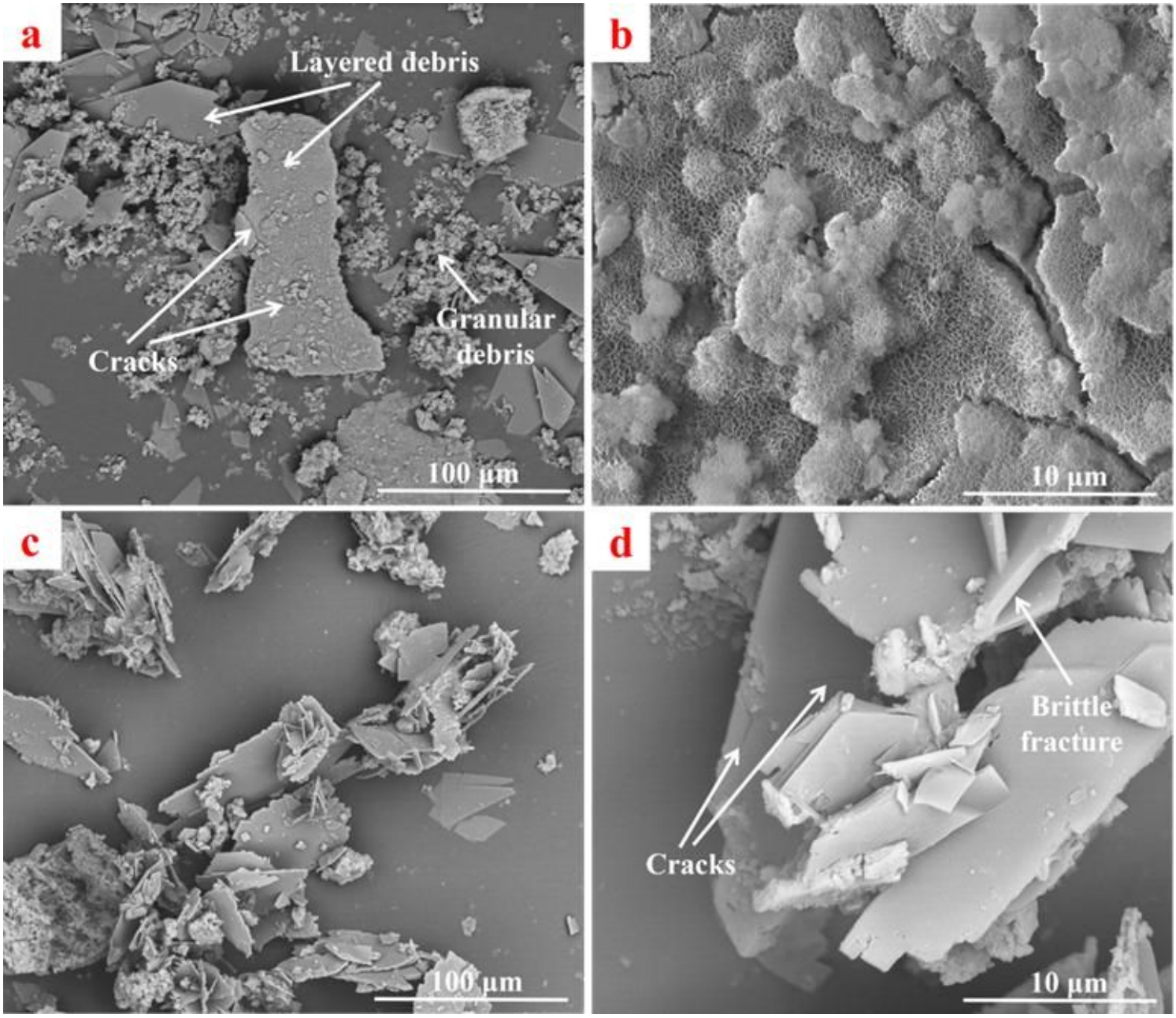

Figure 14

(a-d) Microscopic morphologies of wear debris generated during the friction test.

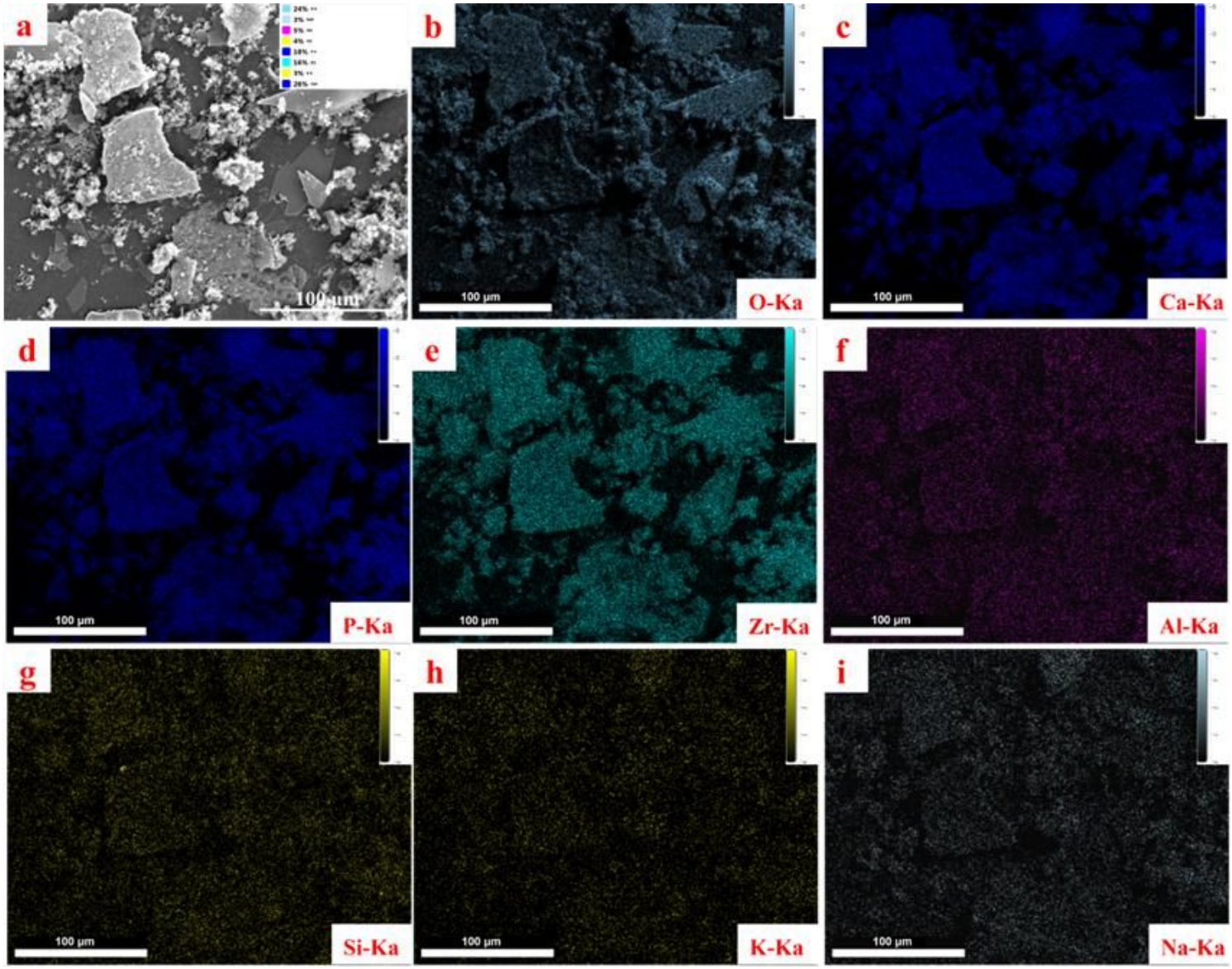

Figure 15

(a) Microscopic morphologies of wear debris; (b-i) Distribution of various elements of wear debris in this area.